Respiratory Physiology & Neurobiology 163 (2008) 100–110

Contents lists available at ScienceDirect

Respiratory Physiology & Neurobiology

journal homepage: www.elsevier.com/locate/resphysiol

Mechanics of airflow in the human nasal airways

D.J. Doorly[a,*], D.J. Taylor[a,b], R.C. Schroter[b]

[a] Department of Aeronautics, Imperial College London, Exhibition Road, London SW7 2AZ, UK
[b] Department of Bioengineering, Imperial College London, London SW7 2AZ, UK

ARTICLE INFO

Article history:
Accepted 30 July 2008

Keywords:
Nasal airways
Computational biomechanics
Physiological flows
Particle image velocimetry

ABSTRACT

The mechanics of airflow in the human nasal airways is reviewed, drawing on the findings of experimental and computational model studies. Modelling inevitably requires simplifications and assumptions, particularly given the complexity of the nasal airways. The processes entailed in modelling the nasal airways (from defining the model, to its production and, finally, validating the results) is critically examined, both for physical models and for computational simulations. Uncertainty still surrounds the appropriateness of the various assumptions made in modelling, particularly with regard to the nature of flow. New results are presented in which high-speed particle image velocimetry (PIV) and direct numerical simulation are applied to investigate the development of flow instability in the nasal cavity. These illustrate some of the improved capabilities afforded by technological developments for future model studies. The need for further improvements in characterising airway geometry and flow together with promising new methods are briefly discussed.

1. Introduction

In all mammals, the upper airway is the portal to the respiratory system and all respired air passes through it on both inspiration and expiration. The upper airway is a complicated structure comprising the mouth and nasal passages placed in parallel, with the nose itself containing two parallel pathways for airflow. Virtually all mammals are obligatory nose breathers; however, at other than relatively low respiratory flow rates, humans and other primates usually breathe preferentially via the mouth (Proctor, 1986). Ventilation is not only cyclical within the upper airway, but usually unequally divided between the two nasal cavities, with the bias of flow alternating between sides over a period of time – the nasal cycle (Eccles, 2000) – that is orders of magnitude larger than a single respiratory cycle. Within the passages of the airway, flow is thus time dependent on both long and short time scales.

The gross architecture of the nasal cavities varies considerably between species (Negus, 1958) for many possible reasons, but particularly to accommodate differing head and jaw shapes associated with eating demands. Consequently, the internal airflow conditions vary considerably between species and in order to understand the details of the airflow and transport properties in the human nose it is important to focus studies explicitly on the human.

The principal physiological function of the nose is to heat and humidify inhaled air (see review in this issue by Elad et al., 2008) and remove noxious materials from the air stream, protecting the delicate distal pulmonary structures. The nose also contains the olfactory apparatus to enable smelling of substances for beneficial or defence purposes (Proctor, 1977). Summary descriptions of the anatomy, physiology and function of the human nasal airways may be found in many works, see for example Mygind and Dahl (1998). The comprehensive text of Lang (1989) includes numerous images of dissections of the airways, compilations of the dimensions of notable anatomical features, and descriptions of variations in morphology.

The technical challenges posed by the task of obtaining detailed, spatially resolved, *in vivo* measurements of the conditions within the nasal airways have yet to be overcome. This is due, not only, to the tortuous geometry of the passages, their narrowness and biological responsiveness to touch, but because any inserted probe is likely to cause perturbations in the flow and introduce experimental artefact. *In vivo* measurement of functional parameters, such as pressure drop, humidification or noxious gas uptake, is essentially restricted to global information based on measurements up- and down-stream of the airway. Internal details are interpreted from this data; however, the complexity of the conduit morphology means that such implied distributed information is based on surmise.

To improve our understanding of nasal function, it is necessary to undertake model studies in which experimental exploration of distributed function can be made explicitly. However, modelling

* Corresponding author. Tel.: +44 207 594 5049.
E-mail address: d.doorly@imperial.ac.uk (D.J. Doorly).

1569-9048/$ – see front matter © 2008 Elsevier B.V. All rights reserved.
doi:10.1016/j.resp.2008.07.027

introduces simplifications which may lead to uncertainty or inaccuracy in translation of the findings back to real life. Both physiologists and modellers need to be fully aware of the shortcomings of modelling in order to make properly informed interpretations of the information obtained in such studies.

The aim of this review is to provide a critical evaluation of issues involved in modelling airflow in the human nose. The nature and quality of experimental data obtained via model studies are considered, and the potential of newer techniques to improve specific aspects of modelling are discussed. Rather than attempting an exhaustive literature critique, references are made frequently to recently published papers containing useful, broad, critical reviews of a particular topic, or which provide an account of the application of particular techniques, that may be used to explore the field further.

2. Model definition and production

Two generic groups of models are considered in this review:

- Physical models – life size, or enlarged – (including: Proetz, 1951; Swift and Proctor, 1977; Girardin et al., 1983; Hornung et al., 1987; Hahn et al., 1993; Guilmette et al., 1998; Horschler et al., 2006; Hopkins et al., 2000; Weinhold and Mlynski, 2004; Kim and Chung, 2004; Kim et al., 2006; Taylor et al., 2005);
- Computational models—(including: Keyhani et al., 1995, 1997; Subramaniam et al., 1998; Horschler et al., 2003; Zhao et al., 2006; Kleven et al., 2005; Zhang and Kleinstreuer, 2004; Lindemann et al., 2004; Naftali et al., 1998; Wexler et al., 2005; Shi et al., 2006, 2007; Franke et al., 2005; Doorly et al., 2008b; Wen et al., 2008; models of pathological airways include Garcia et al., 2007; Lindemann et al., 2005a,b).

The creation of any model, either physical or computational, requires first the identification and definition of the airway boundary. In reality, the airway boundary is time varying, possibly compliant at elevated flow rates and covered for the most part by a thin film of mucus. Furthermore, structures outside the nasal cavity itself affect the flow dynamics within it; during inspiration, the shape of the external nose influences flow entering the nares, whilst during expiration, the airway geometry below the nasopharynx is impressed on the exhaled flow. No model has yet attempted to incorporate fully all these features.

Moreover a wide variety of nasal morphologies exists, so that even an individual perfectly realistic model can only provide partial information. A good example of such variability is the transition between the nasal vestibule and the nasal cavity – the nasal valve – which normally corresponds to a minimum (sometimes denoted CSA-min) in the curve of cross-sectional area (CSA) variation versus flow path length (Fig. 1). The degree and the location of the maximal restriction are not fixed (c.f. Cole, 2000) as erectile tissues are found on both turbinates, and the septum, allowing the geometry to vary due to mucosal engorgement. The degree of contraction imposed on the flow at the nasal valve is known to be an important determining factor of both overall resistance and the nature of the cavity flow (c.f. Schreck et al., 1993; Taylor et al., 2008a), and should therefore be quoted in all model studies. Typical *in vivo* values and ranges of the valve area in healthy adults are:

(a) Numminem (2003) – quoting Márquez Dorsch et al. (1996) – using acoustic rhinometry (AR) on Caucasian subjects, give a non-decongested mean area of 0.68 cm^2 (range 0.44–1.17 cm^2), versus a decongested mean of 0.78 cm^2 (range 0.46–1.23 cm^2);

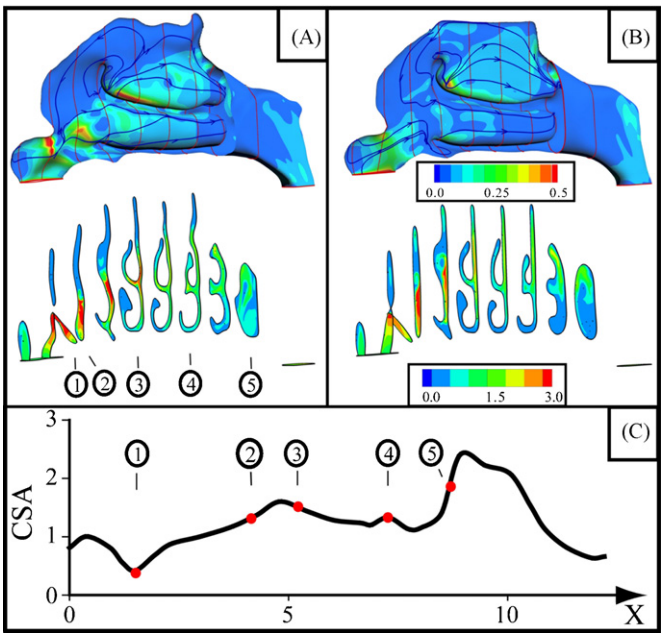

Fig. 1. Models of the nasal airway, both of an anatomical replica (A) and intentionally simplified (B). The distribution of wall shear stress (Pa) is depicted in the flooded contours and the direction of near wall flow is indicated using surface streamlines. Beneath each model, slices through the computational domain depict the shape of the airways and distribution of velocity ($m\,s^{-1}$) for a constant flow rate of 0.1 $L\,s^{-1}$. (C) Depicts a 2D plot of the variation in cross-sectional area, CSA (cm^2), with inter-centroid distance, *X* (cm), for both geometries. *Note*: the locations of the slicing planes are indicated for later reference; slices 1 and 5 denote the location of the nasal valve and opening to the nasopharynx, respectively.

(b) Cakmak et al. (2003), compared nasal valve areas evaluated by AR and by CT in 25 adults, decongested prior to examination; using AR they found the minimum area to range from 0.46 cm^2 to 1.13 cm^2, whilst with CT, the range was 0.54–1.21 cm^2;

(c) Shaida and Kenyon (2000), using AR quote a mean valve area of 0.63 cm^2, and a mean location as approximately 2.3 cm from the external naris, along the acoustic (effectively mean flow) path.

Both inter-population and inter-subject variations have been found. For instance, adaptation to climate is widely regarded to be a cause of underlying differences in nasal form between individuals of differing ancestral origin (*e.g.* Carey and Steegmann, 1981). Ohki et al. (1991) compared measurements of nasal airway resistance in different racial groups and more recently Suzina et al. (2003) reported corresponding measurements in a cohort of 85 non-Caucasian (Malay) subjects. Churchill et al. (2004) observed considerable random variations in morphology (such as relative size of the nasal valve, naris orientation and degree of projection of the turbinates) in a limited study of 10 Caucasian individuals.

The variations in three-dimensional morphology resulting from the nasal cycle have yet to be mapped. Furthermore, in addition to intra-individual temporal variations between left and right sided noses due to the nasal cycle (Eccles, 2000; Hanif et al., 2000), transient variations in nasal airway morphology, which might influence physiological mechanics, may also occur due to flow limitation at higher inspiratory rates. Using acoustic rhinometry coupled with posterior rhinomanometry, Fodil et al. (2005) reported transient, regionally averaged variations in passage area at high inspiratory rates. Aside from the obvious external alar collapse, they draw attention to collapse deeper within the airways; differences in fixed versus compliant airway geometries were less than 20% at lower flow rates (inspiratory pressure drops of less than 30 Pa).

Even with the assumption of a rigid airway, the tasks of defining and reproducing a reasonable constant geometry are challenging due to the anatomical complexity. A straightforward route followed by previous studies either used cadaveric noses directly, or involved casting of cadaver noses; the casts were then used as a master upon which to mould a replica of the original structure. Internal flow conditions were studied using a range of techniques (Proetz, 1951; Swift and Proctor, 1977; Girardin et al., 1983; Hornung et al., 1987; Simmen et al., 1999; Churchill et al., 2004).

Whilst cadaver-based models are relatively easy to create, post-mortem specimens suffer inevitably from uncontrollable tissue shrinkage which renders the airways excessively patent, and possibly distorted. Plastination (von Hagens et al., 1987) is a newer form of preservation in which the dehydration procedure (freeze substitution in acetone) is claimed to result in less than 10% shrinkage (from plastination of brain tissue, Schwab and v Hagens, 1981). This unverifiable estimate is relied on by Croce et al. (2006) to predict mucosal shrinkage for a plastinated specimen. Furthermore, such models are frequently opaque and their 1:1 scale hampers detailed flow measurement.

Rather than relying on such *ex vivo* models, geometry definition based on *in vivo* information is preferable and presently most studies, be they computational or using physical models, are based on data derived from *in vivo* images. Currently, CT, and to some extent MR, imaging of the head to create digital slice images of a subject's nasal topology are the preferred modalities. These slices are then used to delineate the airway boundaries.

Automated procedures for translating image-derived data to an airway boundary for subsequent use in computational modelling or physical model manufacture are now widely applied and detailed elsewhere (*e.g.* Hopkins et al., 2000). However, it is impossible to fully automate the key process of image segmentation, and significant manual user intervention is required. Reviewing the airway geometry in both axial and coronal reconstructions by an expert helps in the manual decision-taking process (*e.g.* Schreck et al., 1993), but the effects of intra- and inter-operator variability need to be considered (Doorly et al., 2008b; Taylor et al., 2008b).

Importantly, the discrete data set of successive sliced nasal wall boundaries produces an ill determined, stepped boundary in all planes. The significance of this loss of resolution must be considered carefully in the context of the experimental objectives (Kleven et al., 2005; Gambaruto, 2007; Gambaruto et al., 2008). Moreover to construct a smooth-walled model, data points must be linked using an arbitrary smoothing algorithm to create a continuous surface. Conventional smoothing (*e.g.* Kobbelt et al., 1998) is known to generate volume shrinkage, particularly in regions of high curvature that are commonplace within the nose; local curvature-adapted smoothing is therefore advantageous (Gambaruto et al., 2008). The departure of the smoothed boundary from the original data should in any case be monitored.

Further errors are likely to occur in the production process of any physical model (*e.g.* by rapid prototyping) and need to be fully assessed. Large-scale errors are manifested as distortions of the geometry, for example by under- or over-penetration of the airway boundary during the cast preparation or filling, or distortion of the mould. At the small-scale, artefactual irregularity of the surface depends on the finish achieved during production. Imaging the physical model by CT at a higher resolution than the original data provides a useful assessment of fidelity (Doorly et al., 2008a).

Physical and computational models have, to-date, almost universally restricted the boundary of the flow domain. Various modifications to the physiological geometry near the outflow boundary are common, ranging from truncation before the passageway curves into the nasopharynx (Hahn et al., 1993), to a rudimentary nasopharynx (*e.g.* Naftali et al., 2005), or a semi-realistic merging of the bilateral streams in the nasopharynx (*e.g.* Kim and Chung, 2004). Manufactured models are generally the more restricted, for instance to just the bilateral airways (Kim et al., 2006), or to a unilateral airway with some form of tube inlet (*e.g.* Kelly et al., 2004a,b; Weinhold and Mlynski, 2004; Taylor et al., 2005). The septum is frequently falsely extended in unilateral models (*e.g.* Schreck et al., 1993; Hopkins et al., 2000); but, visualisation studies employing both split and full-width nasopharyngeal regions for a unilateral airway definition have not revealed significant differences in flow behaviour in the main cavity for inspiratory flow (Doorly et al., 2008a). However, the mixing and pressure loss in the nasopharyngeal region cannot be accurately represented using such an artificial boundary, and in general, the effects of any boundary condition modifications need to be considered carefully.

For inspiratory modelling, it is important to consider whether to apply either a blunt, or a fully developed tube, velocity profile at the naris, or, if the external nose and the face should be included (Taylor et al., 2008a). Incorporating the external nose and at least a local portion of the face not only replicates the physiological situation, but for computational studies furnishes additional information, for example the spatial origin of inspired air. The most extensive domain used to date is probably that in the plastinated specimen of Croce et al. (2006), which encompassed the bilateral nasal airways and part of the face. Non-physiological inflow conditions (with a few exceptions such as Croce et al., 2006; Doorly et al., 2008b) have been applied to all physical and computational models, using typically a developed pipe flow (of varying orientation at the naris), or a plug flow.

Having defined the extent of the modelled domain, the choice may be made to investigate flow in either an accurately replicated 'person-specific' anatomy, or an idealised configuration. Such idealisations of the nasal architecture may be necessary to facilitate model construction and experimentation or for computational convenience (*e.g.* smooth or structured multiblock mesh creation—Horschler et al., 2003). Other studies (*e.g.* Elad et al., 2006) have taken an objective rational approach to simplification leading to far greater degrees of idealisation. Gross features of the nasal cavity and turbinates are represented by relatively primitive structures intended to simulate reality. The flow characteristics determined in such geometries are then compared with limited studies in more realistic anatomical geometries (Naftali et al., 2005) to identify the principal properties of the flow. Intentional simplification moreover allows the sensitivity of flow to geometry definition to be studied in a systematic and rational way (Gambaruto, 2007; Gambaruto et al., 2008; Taylor et al., 2008b).

An illustration of intentional simplification is shown in Fig. 1. The right nasal airspace is shown faithfully reconstructed (Fig. 1A) and in simplified form (Fig. 1B). The viewpoint is inwards from the septal wall, with that wall removed to reveal the turbinates and surface streamlines at a steady inspiratory flow at 0.1 $L s^{-1}$. In the simplified model (Fig. 1B) the bounding contours have been altered whilst maintaining the original variation in passage cross-sectional area of the faithful model along an assumed mean flow path (Fig. 1C). In the lower panels of Fig. 1A and B, the local in-path or effectively axial velocity distributions within the nasal conduits can be seen at each of the coronal cross-sections identified in the upper panels.

When deciding on the appropriate definition and form of any physical or computational model, whether replica or idealised, the implications of all real variations in geometry should be carefully distinguished from the uncertainties associated with replicating a specific anatomy. Moreover, regarding simplified models, until the functional relationships between architecture and flow are better understood, it is necessary to acknowledge that the introduction

of simplifying changes may introduce unintended, but significant, artefactual effects.

Currently there is no agreed rational process by which individual models can be described or different models compared. Systematic analysis and comparisons of different model studies would provide a more informed evaluation of the relationship between structure and function. To accomplish this, it would be helpful in future if:

(a) models could be described in a compact hierarchical manner;
(b) methods are established to characterise and compare different anatomies;
(c) rational methods are established to extract key geometrical features.

A possible way forward to achieve this would be to use alternative means to define and characterise geometry (*e.g.* Gambaruto, 2007).

3. Airflow studies

3.1. General flow properties

The patterns of airflow within the nose can be determined, in principle, by both experimental and computational methods. However, the two approaches have differing strengths and weaknesses that lead to their being strongly complementary, and in order to understand the more detailed and time varying processes, it is invaluable to compare results of the two approaches in similar geometries.

Visualisation, though not quantitative, potentially provides a powerful, rapid and flexible means to investigate nasal airflow dynamics. Both smoke particles in air-filled models (*e.g.* Simmen et al., 1999), and dye filaments in water or other liquid-filled models have been employed (*e.g.* Weinhold and Mlynski, 2004; Taylor et al., 2005). The disadvantage of smoke is not only that it is very difficult to image, but the effective slowing down of the dynamics by an order of magnitude gained with a liquid allows even rapid transient dynamics to be captured photographically.

Fig. 2A shows the application of dye visualisation to reveal overall patterns of flow in the nasal cavity at a steady inspiratory rate of 0.1 L s^{-1}. Readily identifiable features include the large recirculation in the upper anterior cavity, the deflection of flow impacting on the middle turbinate, and the turning and mixing of the air stream as it exits into the nasopharynx. The laminar character of the flow is obvious, though dye filaments passing close to a surface can become widely dispersed.

Experimental measurements of velocity have been obtained using (point-wise) hot-wire anemometry (Hahn et al., 1993), and more recently with (planar whole field) digital particle image velocimetry (PIV) techniques (*e.g.* Hopkins et al., 2000; Kelly et al., 2004a,b; Kim and Chung, 2004; Doorly et al., 2008a,b). PIV provides a rapid, convenient means to achieve whole field data, and to assess the accuracy of computational predictions—the use of PIV in the nose is covered extensively in the companion review in this volume (Chung and Kim, 2008).

Whilst direct measurements of velocity in life sized, and scaled up, models of the nose are useful, there are many associated experimental difficulties which have contributed to the attraction of using computational modelling methods. A general overview of some issues in applying computational fluid dynamics (CFD) techniques to modelling nasal airflow is given in the review of Bailie et al. (2006).

Although both finite element and finite volume solution methods for the governing flow equations are well-developed, mesh generation in the narrow and complex nasal passages still poses major difficulties. The density of the mesh should be sufficient to resolve sharp gradients and although block-structured meshes have been used in some cases (Keyhani et al., 1995; Horschler et al., 2003, 2006), it is very difficult to refine such meshes in the complex nasal passages, and this has largely precluded their use in anatomically accurate models. Hybrid meshes with multi-layered prismatic wall elements are now common (*e.g.* Zhao et al., 2004), with the first prism layer located a small fraction of the passage width away from the wall (*e.g.* Doorly et al., 2008b). Overly rapid transitions in mesh size can degrade the solution, and assuring continuous, smooth resolution of flow everywhere leads to large numbers of elements, with associated computational time and cost. For example, simulating the development of flow unsteadiness in regions away from the wall, such as the margins of the inspiratory jet, require fine resolution, with at least 4 million elements required for a half-nasal model (Taylor et al., 2008b).

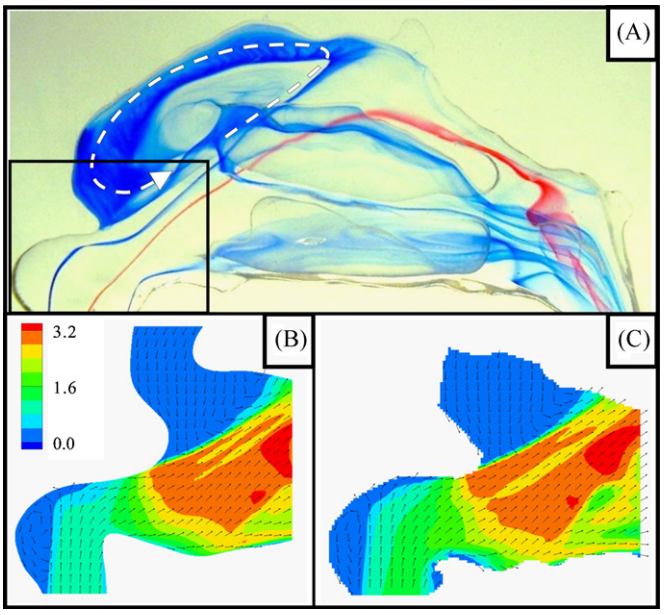

Fig. 2. Comparison of experimental and computational simulations at a constant inspiratory flow rate of 0.1 L s^{-1} obtained in the anatomical replica model shown in Fig. 1A. (A) Depicts neutrally buoyant dye filaments, metered into the flow (upstream of the model nostril to the bottom left of the figure) which highlight the gross flow patterns and steadiness as well as the large anterior recirculation region (identified using a dashed arrow). (B) and (C) From a mid-sagittal slice through the anterior part of the nasal airway, corresponding to the region in the box demarcated in (A). They show a comparison between computational prediction (B) and PIV measurement of the velocity field (C). Flooded contours and uniformly sized vectors depict, respectively the in-plane velocity (m s^{-1}) and direction, and indicate the structure of flow converging through the nasal vestibule, which forms a high-speed jet, driving the recirculation shown in (A).

An active and promising research area is the development of numerical procedures which avoid the difficult mesh generation stage. Few such studies relating to the nasal airways have yet been performed, though Finck et al. (2007) have computed flow in the geometry of Horschler et al. (2003), and obtained close agreement with the earlier results.

Wolf et al. (2004) provide a concise review of the findings of earlier mechanics studies of the patterns and distribution of airflow in the nasal cavity, including sketches of mean flow path lines or the velocity field during inspiration and expiration, which they adapted from the studies of Proetz (1951), Proctor (1986), Hahn et al. (1993) and Brucker and Park (1999). Many other works illustrate the velocity field and/or pathline patterns in various nasal airway models, using images derived from visualisation, computation or

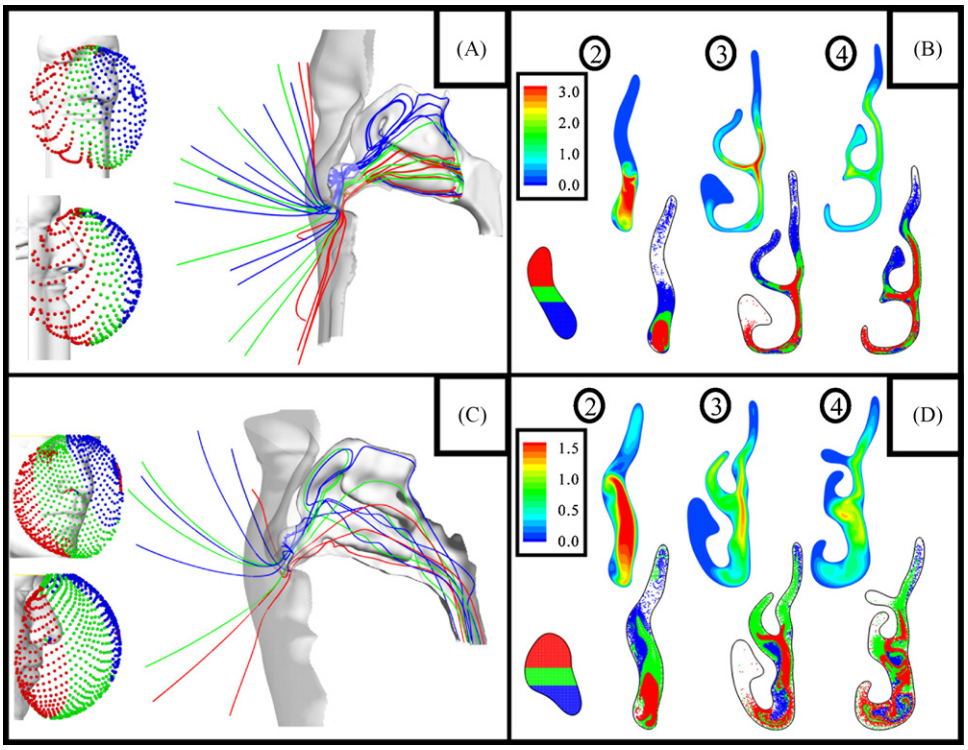

Fig. 3. Computational simulations at a constant inspiratory flow rate of 0.1 L s^{-1} have been exploited to yield massless particle tracks and planar velocity slices for two nasal geometries: the anatomical replica of Fig. 1A (A and B) and a highly decongested replica geometry (C and D). In (A) and (C), 10,000 massless particles, initially seeded at the nostril, were tracked through the computational domain; (a) tracking forwards in time to yield fluid trajectories and flow partitioning within the nasal cavity and (b) tracking backwards (for a single breath, 0.5 L) to yield the volume and origin of inhaled air as delineated by the particle clouds shown to the left in each figure. Particles are colour-coded by their coronal location at the nostril (as indicated in (B) and (D)). In (B) and (D), slice data for each geometry depicts velocity magnitude (m s^{-1}) and the location at which each particle track passes through each slice (slices are labelled 2, 3 and 4, as shown in Fig. 1A). The initial particle distribution at the nostril of each geometry is also shown (blue particles are situated at the tip of the nostril). (For interpretation of the references to color in this figure legend, the reader is referred to the web version of the article.)

experimental measurements. Significant among these are Schreck et al. (1993), Keyhani et al. (1995, 1997), Subramaniam et al. (1998), Hopkins et al. (2000), Horschler et al. (2003, 2006), Kim and Chung (2004), Weinhold and Mlynski (2004), Zhao et al. (2004), Naftali et al. (2005), Croce et al. (2006), Doorly et al. (2008a,b), Gambaruto et al. (2008), Taylor et al. (2008a,b) and Wen et al. (2008).

Direct comparisons of computational predictions with detailed experimental measurements of the flow field are relatively rare. Keyhani et al. (1995) demonstrated reasonably good agreement between numerically predicted velocities and those measured using a hot film probe in a 20-times scale unilateral nasal model.

Fig. 2 also shows a comparison between computational prediction (Fig. 2B) and PIV measurement of the velocity field (Fig. 2C) in the region indicated by the rectangle in the dye visualisation study (upper panel) at the same steady flow rate of 0.1 L s^{-1}. Both sets of results (obtained by us) provide details about how the inspired flow converges through the nasal vestibule and its subsequent injection as a high-speed jet into the main cavity and the driving of the extensive upper zone of flow recirculation shown up by the visualisation study. The close agreement between the features shown by the differing modalities clarifies the nature of the flow in this region, including the sharp margin of the inspiratory jet.

It has generally been shown that the flow in the nasal cavity is largely determined by the inflow condition, the geometry of the cavity and the size and orientation of the internal nasal valve. Although each is important, the internal nasal valve represents a localised region that model studies have shown to profoundly influence all the principal characteristics of the airflow, including the pattern of streamlines, flux to the olfactory cleft, particle deposition and overall resistance to flow. Whilst all studies indicate that the inspiratory flow through the constriction at the internal nasal valve is well-ordered, the pattern of flow downstream on entering the main cavity varies markedly. Thus the results for some model geometries display pronounced regions of recirculation in the anterior cavity, whilst this feature is absent in others. Likewise, the distribution of flow about the turbinates varies, though it is generally relatively slow in the upper meatus and in the olfactory cleft region.

Computations which incorporate the external face as part of the modelled domain provide the most realistic physiological inflow description (Fig. 3). The errors associated with incorrect inflow specification have been quantified (Taylor et al., 2008a) with appreciable differences being found between simulations using a physiological inflow and a blunt profile. They showed that, whilst the contraction and orientation of the nasal vestibule reduce the influence of the inflow profile, the choice of inflow results in significant differences in quantities such as airflow to the olfactory cleft. Moreover, specification of a blunt velocity profile induces fresh boundary layer growth from the naris with a slight increase in overall pressure loss.

In Fig. 3, particles arriving at the right naris are traced back to the external location from which they would originate, in a single, steady inhalation. Marker particles are assigned one of three colours, depending on their position in the anterior–posterior direction at the nostril entrance. The velocity and the distribution of particles crossing three corresponding sequential coronal slices (locations as specified in Fig. 1) are shown for the anatomical replica of Fig. 1A (Fig. 3A and B) and a replica, but highly decongested geometry (Fig. 3C and D). Comparing the distribution of particles, the

relative lack of 'mixing' (strictly stirring, since diffusion is not incorporated) within the cavity is evident. The colour coding shows that flow reaching the upper cavity predominantly passes through the anterior part of the nasal vestibule, as reported previously (Keyhani et al., 1995; Zhao et al., 2004). Fig. 3A and C also shows that the upper cavity flow streams originate from directly in front of the nose, rather than from the lateral or vertical margins.

Both the velocity of the airflow, and its spatial and temporal variations, very near the wall and the related shear rate, or shear stress (WSS), at the wall are important quantities in relation to many physiological processes, for example pressure drop through the nose, particle deposition and exchange processes at the wall. Wall shear has also been identified as a putative agent for mechano-transduction between the airflow and the nasal epithelium as discussed by Elad et al. (2006).

Computational modelling enables the WSS, and other physiologically related parameters that are difficult or impossible to measure directly, to be deduced. The upper panels of Fig. 1A and B show the distribution of WSS on the exposed lateral wall. Colouring, indicating the magnitude of WSS at an inspiratory flow rate of 0.1 L s^{-1}, reveals zones of high wall shear in the vicinity of the nasal valve where flow is squeezed through the narrowed space, and the anterior portions of the middle and inferior turbinates where impingement of the airstream on the fronts of the turbinates leads to fresh boundary layer development; lower values of WSS are found in the region of the olfactory cleft (below the 'w'-shaped depression in the roof of the cavity). The notable marked inhomogeneity in WSS reveals that the complexity of nasal airflow is intimately associated with the geometric complexity.

3.2. Unsteadiness of the flow

The type of flow regime that exists over the breathing cycle, particularly through the inspiratory phase, significantly affects function—from the overall pressure losses, to the transport of air borne species and even possibly the stimuli transmitted to the nasal mucosa and epithelium.

Despite extensive earlier work, there is still uncertainty with regard to two basic questions in modelling nasal airflow. Can the flow be modelled as steady and is the flow laminar, transitional or turbulent? Previous studies suggest that the answers to these questions are not clear cut. The type of breathing (*e.g.* steady and quiet slow breathing vs. rapid sniffing) is important, with a particular anatomy tending either to increase or decrease flow stability. Clearly the real flow is not steady, so the question is whether modelling the mean flow as a steady process, or as a series of quasi-steady flows is sufficient to characterise the airflow and the physiological functional performance of the nose.

3.2.1. Phase related variations

For quiet breathing at a frequency (f) of 15 breaths per minute (using characteristic scales for (i) time ~ equivalent to airway length (L) divided by mean velocity (U), and (ii) the passage radial calibre [$d/2$] = 3 mm) values of the Strouhal (St) and Womersley (Wo) numbers

$$St = \frac{2\pi f L}{U}, \qquad Wo = \frac{d}{2}\left(\frac{2\pi f}{\upsilon}\right)^{1/2}$$

(where υ = kinematic viscosity of air) are less than 0.25 and 3, respectively. This suggests that the quasi-steady approximation is valid, and this view is reinforced by computations which model the inspiratory period as a flow waveform. For example, the results of Shi et al. (2006) reveal only minor differences in the velocity contours at a given flow rate between the accelerating and decelerating portions of the flow waveform. Most studies have gone further than this and assume a steady flow as representative of the 'average' conditions over the entire inspiratory period (*e.g.* Keyhani et al., 1997; Wen et al., 2008). However, a steady mean flow assumption is not suitable for modelling accumulative processes such as deposition (Shi et al., 2006), odorant transfer (Zhao et al., 2004, 2006) or heat transfer (Naftali et al., 2005; Ishikawa et al., 2006) over the cycle. Nor is it suitable when determining how mechanical stimuli, such as surface traction, are transmitted to the nasal epithelium by varying airflow (Elad et al., 2006). The approach taken by Shi et al. (2006) to reduce the computationally demanding cost of fully modelling the inspiratory waveform is interesting; they determined an 'equivalent' steady flow as $0.5(U_{mean} + U_{maximum})$ which effectively reproduced the deposition results obtained by full simulation. However, the effectiveness of such an approach is problem-dependent, and requires validation in each case.

Where hysteresis is manifested over the inspiratory period, a steady state model is certainly inappropriate. In principle, such hysteresis could arise due to fluid dynamic effects (*e.g.* via unsteady separation in the flow in the nose), or for structural reasons (*e.g.* oscillation or displacement of any of the airway walls). Measurements of the pressure-flow relation given by Fodil et al. (2005) display hysteresis, but in that study, very high pressures (300 Pa, 10 cm H_2O) were sustained. They reported that below pressures of 30 Pa, there was little difference in flow predicted by rigid or compliant models. Likewise, the temporal variation of wall shear over the inspiratory period given by Elad et al. (2008) appears symmetric about the point of maximal flow. Therefore at least for quiet breathing, it seems reasonable to disregard hysteresis; however, this may not hold for other regimes such as rapid sniffing.

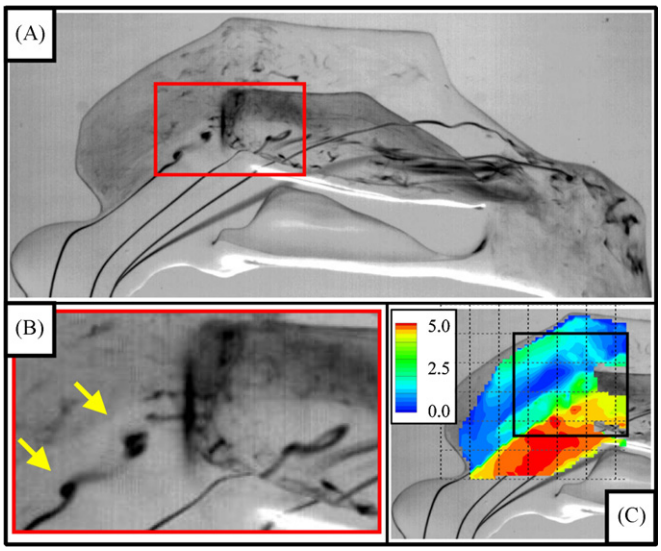

Fig. 4. High-speed dye visualisation and PIV reveals the onset of instability at an increased, effectively unsteady flow rate (~0.2 L s^{-1}) in the simplified geometry of Fig. 1B. (A) (together with the magnified image of the demarcated box in (B)) provides a striking illustration of the shear layer instability at the margin of the inspiratory jet entering the nasal cavity. Flow remains laminar across most of the nasal airspace, though the upper margin of the jet undergoes instability approaching the middle turbinate. Slow motion review of image sequences (captured at an *in vivo* frame rate of ~3000 fps) reveals small amplitude fluctuations in filaments (arrowed in (B)) approaching the stagnation of the inflow jet on the middle turbinate that leads to amplified dispersion; this may give a misleading impression of disturbance amplitude of flow in the upper region of the cavity. The spatial scaling of the disturbance in (B) is directly comparable with that depicted in (C), which shows corresponding PIV measurements of velocity (m s^{-1}), providing a quantitative determination of the sharp interface between the high-speed inspiratory jet (with peak in-plane velocities reaching 5 m s^{-1}) and the slow anterior recirculation region. The demarcated box provides the reference location for the measurements shown in Fig. 5.

3.2.2. Laminar v turbulent flow

Whilst a detailed consideration of mixing and transport processes in the nose, such as delivery of odorants to the region of the nasal cleft and conditioning of inspired air, are beyond the scope of this review, their characteristics depend fundamentally on the nature of the airflow within the nasal cavity, both within the bulk of the airstream and very near the walls. Whether the flow is truly laminar, but possibly disturbed, or turbulent is ultimately key to the understanding of these processes.

At sufficiently low flow rates, airflow is laminar throughout the nasal airways. However, there is uncertainty both as to when departure from laminar behaviour can be expected and how the state of the flow develops from fully laminar to fully turbulent—if indeed the latter stage is ever fully attained. The state is unlikely to change suddenly from laminar to turbulent. Instead, a transition process will occur in which semi-regular, self-sustained oscillatory features appear as disturbances to laminar flow; with progressive increases in flow rate, random, small scale disturbances will develop. Evidence regarding the nature of flow in the nasal cavity has been derived by inference from pressure loss, and directly via hot wire measurements and visualisation in models.

Attempts to determine the flow state in the nose indirectly from the overall pressure loss are hampered by the intricate geometry of the cavity where the opportunity for complex zones of recirculation renders direct comparison with classical correlations for pipe flow questionable. The dimensionless pressure loss coefficient has been found to vary approximately inversely with Reynolds number (*Re*, the classical indicator of transition from laminar to turbulent flow in a given geometry) at low flow rates—reducing to an inverse third power law (Croce et al., 2006) or a constant value (Schreck et al., 1993) at higher flow rates, thus confirming an eventual transition from a fully laminar to turbulent state.

Using hot wire anemometry, Hahn et al. (1993) measured the intensity of velocity fluctuation (ratio of velocity fluctuation to local mean velocity). They concluded that flow in their half nasal model was 'disturbed laminar' at a flow rate of 0.18 L s^{-1}, and turbulent at the higher flow rates studied. However, hot wire studies are difficult to conduct in nose models—in larger models the flow velocities can become very small, whilst access is very difficult in smaller models. Employing conventional PIV methods, Kim and Chung (2004) determined the root mean square (rms) intensity of velocity fluctuations in the nasal cavity, observing high levels where the inspiratory jet entered the cavity from the valve. However, snapshot measurements using conventional PIV techniques are not well-suited to probe the interesting and important unsteady dynamics.

Visualisation has been used frequently to decide whether nasal airflow is laminar or turbulent (*e.g.* Simmen et al., 1999; Churchill et al., 2004). Although the technique illustrates well overall features

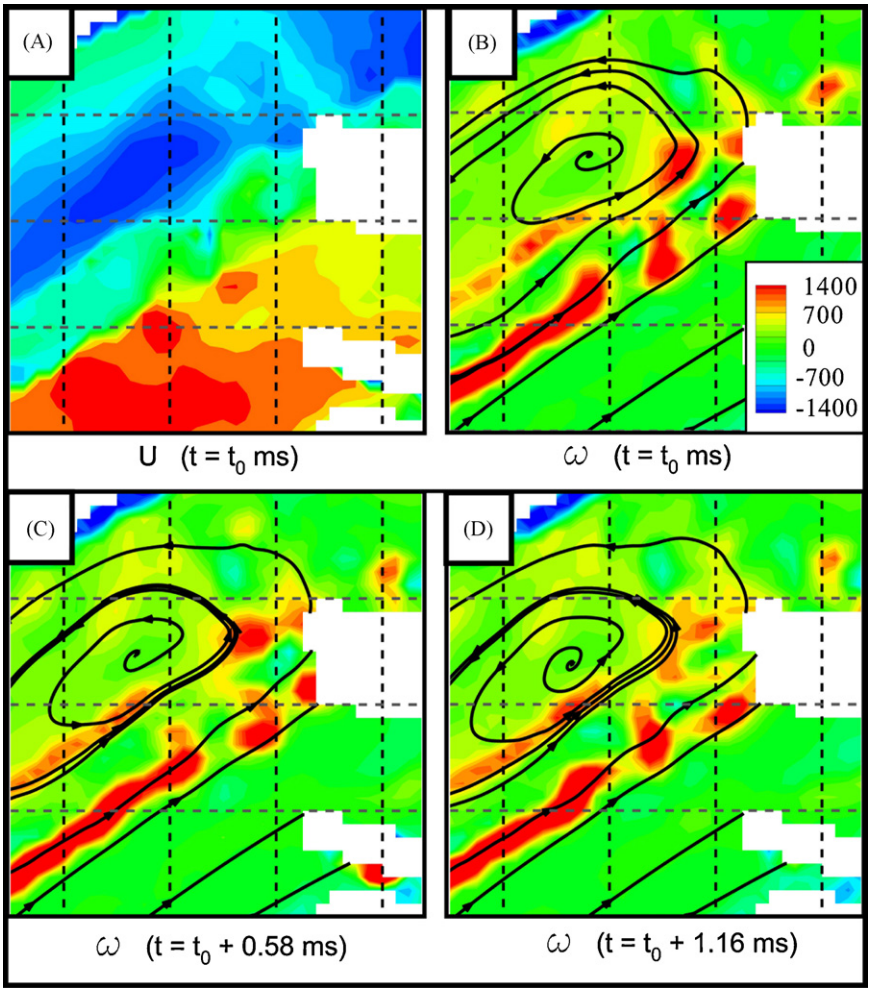

Fig. 5. Time-resolved PIV for a flow rate of ~0.2 L s^{-1} in the simplified geometry of Fig. 1B. The magnified location and orientation of the PIV measurements is indicated in Fig. 4C. Flooded contours of in-plane velocity magnitude (U, m s^{-1}), and vorticity (ω, s^{-1}) at an instant (t_0) are shown in (A) and (B). Successive (0.58 ms time lapse) instantaneous vorticity fields show the evolution and periodic nature of the instability (C and D). The movement of the features can be seen by observing their displacement relative to the broken grid.

such as zones of recirculation, it can be misleading. Even minor laminar flow disturbances in complex configurations can induce rapid dispersion which may be confused with turbulent mixing. Assessment of the flow state needs to be based on visualisation techniques that are capable of revealing the complexity of the dynamics and to distinguish early instability from fully developed turbulence.

Dye visualisation images showing the development of flow instability are given by Doorly et al. (2008a,b) at flow rates up to $0.17\,L\,s^{-1}$. Fig. 4A (together with the magnified image in Fig. 4B of the highlighted region) provides a striking illustration of the shear layer instability at the margin of the inspiratory jet entering the nasal cavity at a slightly higher flow rate of $0.2\,L\,s^{-1}$. The roll up and shedding of periodic structures in the vicinity of the middle meatus can be clearly seen. It is particularly noteworthy that the third dye filament from the top, which bypasses the middle turbinate, remains largely unaffected by the shear instability; this indicates relatively undisturbed laminar flow within much of the cavity. Fig. 4C shows an instantaneous snapshot of PIV measurements of velocity, providing a quantitative determination of the sharp interface between the high-speed inspiratory jet and the slow anterior recirculation region. In Fig. 5, a series of time-resolved high-speed PIV images (landmarked in Fig. 4C) focus on the edge of the shear layer. The in-plane velocity (U, $m\,s^{-1}$) and in-plane vorticity (ω, s^{-1}), shown in Fig. 5A and B at an arbitrary time denoted t_0 after the establishment of a steady inspiratory flow of $0.2\,L\,s^{-1}$. The images in Fig. 5C and D chart the oscillation and break up of the concentrated vorticity into discrete structures.

4. New research directions

The numerous model studies performed to-date have contributed greatly to our understanding of how the nose functions, but it is also clear that there are significant gaps in this knowledge. Outlined briefly in this review is some recent progress in the areas of: (i) definition of the model airway, (ii) the effect of flow instability on wall shear stress and (iii) sniffing, which it is anticipated will play a significant role in future developments of nasal airway modelling.

4.1. Definition of the model airway

The issues of defining airway geometry and its variations have, as yet, scarcely been addressed in a rational way in model studies. The important causes of variability are twofold. First is the issue of uncertainty where, for example, different operator choices in the image segmentation process lead to variation in the delineated airway geometry. The second reflects 'genuine' physical variability, both intra- and inter-individually. For both reasons, compact, hierarchical descriptions of the complex geometry of the nasal airways are needed to characterise how form and function are related.

Various alternative techniques for the representation of nasal airway geometry have recently been introduced including skeletonisation, Fourier descriptor contour representation and harmonic mapping (Gambaruto, 2007). The technique of skeletonisation in 2D was introduced by Blum (1967) and is commonly used in image processing and machine vision, *e.g.* Sonka (1995), Jain (1988), and Weeks (1996). In nasal airway skeletonisation (summarised by Doorly et al., 2008b), the surface of the lumen is decomposed into a stack of branched 'skeleton' curves, and associated thickness distribution; the decomposition is reversible, with the airway surface recoverable via implicit function reconstruction techniques (*e.g.* Gambaruto et al., 2008). Given that the underlying structure of the nasal airways is for the most part axially invariant, regional variations in passage calibre (simulating different states of congestion, or even temporal variations) can be applied without altering the airway 'skeleton'. The process of airway skeletonisation also enables meaningful averaging of topological form and regional passage calibre variation from data corresponding to different subjects. Characteristic topological features could be extracted via Proper Orthogonal Decomposition techniques which are described by Doorly et al. (2008b).

Many alternative representations of the airway geometry, based on a direct, hierarchical description of the lumen boundary are possible, for example using Fourier descriptors for contour representation (Gambaruto, 2007). As with skeletonisation, this provides a means to compare and characterise geometry, and

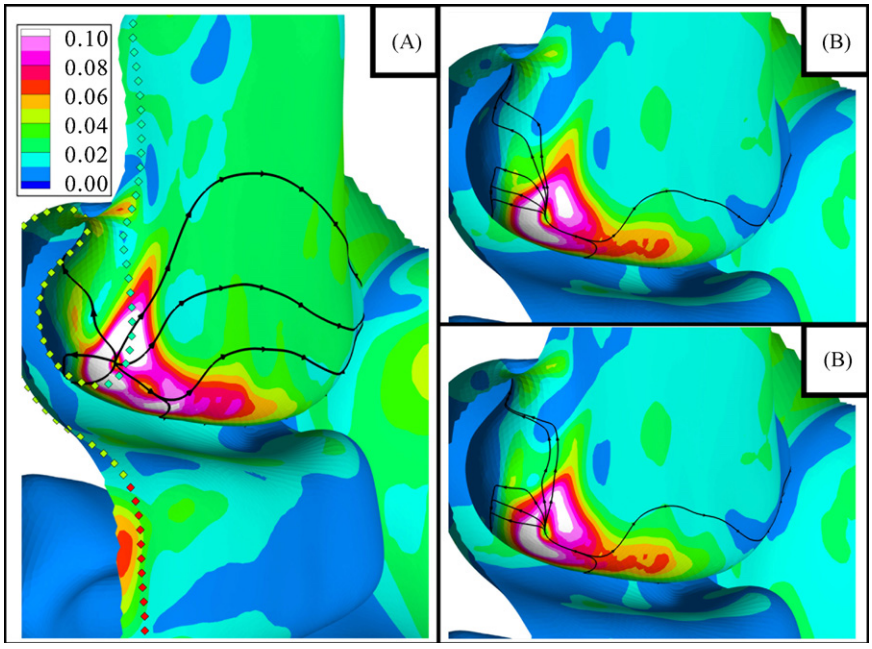

Fig. 6. Computational simulation during inspiration of normalised WSS* distributions in the region of the anterior middle turbinate (WSS is normalised by the dynamic pressure $0.5\rho U_m^2$ – where ρ and U_m are respectively the fluid density and mean velocity at the nasal valve – $2.15\,m\,s^{-1}$ at a flow rate of $0.1\,L\,s^{-1}$). (A) For a flow rate of $0.1\,L\,s^{-1}$; (B) and (C), showing two successive snapshots separated by 0.5 ms, are for the effectively unsteady flow rate of $0.2\,L\,s^{-1}$.

has been applied to investigate the sensitivity of model geometry to small perturbations (Gambaruto et al., 2008). Other general techniques for morphometric analysis may be useful; particularly promising is the formulation developed by Cotter (2008) which is based on variational methods, and to which the reader is referred.

4.2. Effect of flow instability on wall shear stress

The effects of flow instability at the higher flow rates on the impact of the inspiratory jet on the middle turbinate is shown in Fig. 6 where the steady (0.1 L s^{-1}, Fig. 6A) and unsteady (0.2 L s^{-1}, Fig. 6B) flow rates are compared. The relatively high values of the friction coefficient (WSS normalised by the dynamic pressure – $1/2\rho U_m^2$ – calculated at the nasal valve) in the region of the stagnation of the jet on the middle turbinate reflect the growth of fresh boundary layers. The surface streamlines indicate how the flow, deflected about the leading edge of the turbinate, changes in orientation under the different conditions (Fig. 6A and B).

Comparing the two sequential plots (Fig. 6B and C) of friction coefficient at the naturally unsteady, higher flow rate, with that at the lower steady flow rate (Fig. 6A) reveals some interesting phenomena. Firstly, the near equivalence of levels and distribution of normalised WSS, despite doubling of the flow. Secondly, although unsteady shear layer break-up occurs at the margins of the inspiratory jet, the stagnation point of the jet on the turbinate shows little displacement with increasing flow rate.

The small alterations in normalised WSS are quantified in the line plot (Fig. 7B) round the wall on a slice extracted through the computational wall mesh. Colour coded diamond symbols, normalised by perimeter distance, show the shape of the extracted slice (Fig. 7A) and the coloured lined in Fig. 7B indicates position round the contour of the wall. The location of the slice is also shown using the same colour coded diamond symbols in Fig. 6A. The solid lines (red and black represent two instantaneous measurements, separated by 0.5 ms, at the flow rate of 0.2 L s^{-1} and show little notable difference. The blue circular symbols represent the same slice for a flow rate of 0.1 L s^{-1}, these show the same general qualitative structure and patterns of those at 0.2 L s^{-1}.

In contrast, there are striking alterations in surface streamline pattern for the flow being deflected upwards and anteriorly by the anterior head of the middle turbinate. The change in WSS due to a gross increase in flow (a doubling) may represent a low-frequency, quasi-steady alteration, whilst the shear layer instability, as indicated by the changing streamline behaviour, leads to a high frequency variation.

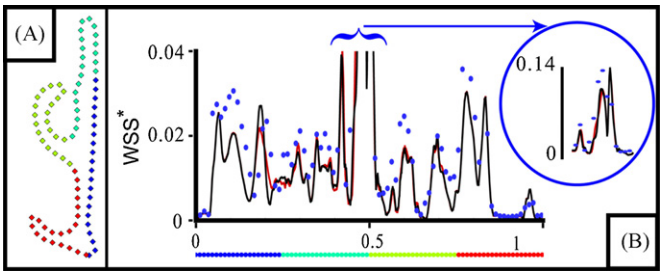

Fig. 7. Distribution of normalised WSS* along the perimeter of the wall for computational simulations described in Fig. 6. The shape of the extracted wall boundary slice is shown, colour-coded by normalised perimeter distance in (A). For reference, the boundary of this slice is also shown *in situ* in Fig. 6A and demarcated by the coloured diamonds. (B) A 2D plot of WSS* distribution extracted from a slice including the stagnation point of flow on the middle turbinate. The black and red lines represent the first and second instantaneous distributions (0.5 ms apart), respectively, at a flow rate of 0.2 L s^{-1}. The blue symbols represent the comparable slice at a flow rate of 0.1 L s^{-1}. The horizontal axis represents normalised perimeter location; shown beneath the 2D plot are the symbols of the unwound perimeter location, corresponding to (A). (Because the peak WSS is nearly an order of magnitude larger than the mean, the peak has been removed and is shown within the blue circled inset.) (For interpretation of the references to colour in this figure legend, the reader is referred to the web version of the article.)

4.3. Sniffing

The dynamics of airflow and transport in sniffing are of increasing interest, particularly from a diagnostic and therapeutic viewpoint. Mild sniffing comprises short sequential bursts of increased inspiratory airflow rate (>0.5 L s^{-1}). The resultant increased pressure drop induces some degree of collapse of the external nose, and probably affects flow transiting the nasal vestibule. Deep sniffing, involving relatively high transient flow rates (probably >1.0 L s^{-1}), produces a marked degree of alar collapse. The time taken to initiate significant airflow velocities in the nose can be very short; our own preliminary investigations using hot wire anemometry indicated that flow can rise significantly well within 40 ms.

Fig. 8A depicts a slice (the same as that of Fig. 4C) through the computational domain showing the in-plane vorticity magnitude (s^{-1}) for an established flow rate of 0.2 L s^{-1}. The amplified instability can be observed in the shear layer, with planar streamlines denoting velocity direction. The formation and rollup of the starting vortex was analysed for a transient linear ramp of flow from 0 L s^{-1} to 0.2 L s^{-1} in 0.1 s—a time scale consistent with a gentle sniff. At the beginning of this sniff, fluid velocities are low and separation of the inspired jet is relatively weak (Fig. 8B). This allows inspired air

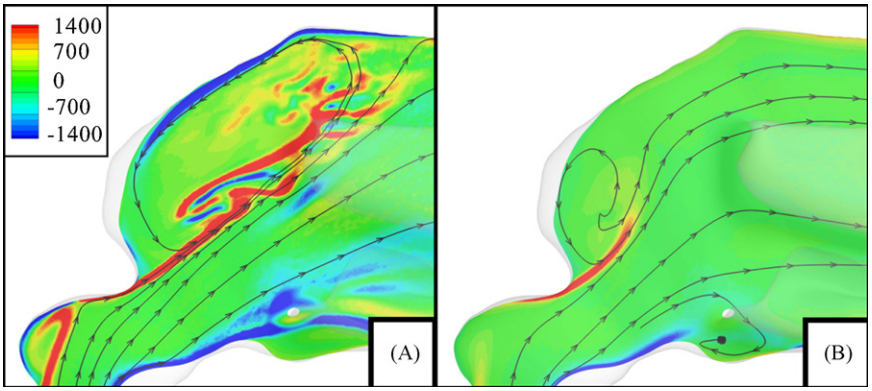

Fig. 8. Computational simulation, in a mid-sagittal slice, of a transient (0.1 ms duration) pseudo-sniff inspiration for the simplified geometry of Fig. 1B. Flooded contours of in-plane vorticity (s^{-1}) and planar streamlines (indicating flow direction) for an established flow at 0.2 L s^{-1} depict the onset of flow instability (A). The starting vortex for a pseudo-sniff (linear ramp from 0 L s^{-1} to 0.2 L s^{-1} over 0.1 s) for an instant in time at 0.04 s can be seen in (B).

to be drawn into the anterior part of the cavity as demonstrated by the streamlines. The growing starting vortex will eventually form (in a time of the order of 0.1–0.2 s) the large anterior recirculation region previously described (Figs. 5 and 8A). The gradual growth of the vortex entrains and mixes inspired air before it is re-released into the jet and convected to the roof of the nasal passageway for olfaction. This pattern of behaviour could possibly play a significant role in olfaction by mixing air-streams from different origins around the external face before they reach the olfactory cleft.

5. Conclusions

The ultimate goal of modelling studies in the field of nasal mechanics must be to shed more light on the underlying physiological processes in health and disease, or to improve the provision of interventional actions from the delivery of aerosolised drugs to functionally based surgical planning. This review of the mechanics of nasal airflow has considered information deduced from model studies in the context of a critical examination of the bases and potential capability of the various model types and experimental approaches. It is intended to be complementary to the reviews of Elad et al. on nasal air conditioning, Chung and Kim on the use of PIV to study nasal airflow and Kleinstreuer et al. on airflow and particle transport processes in this issue.

Advances in imaging capabilities, model production methods, computing power and measurement techniques are all leading progressively to a better understanding of the underlying mechanics and there is strong evidence of translation of advances in other areas of mechanics and modelling to the topic. However, the field has not yet advanced to the point where detailed mechanistic comparisons can be achieved between the model and real environments in ways that fully exploit the technical possibilities.

Exploratory studies of potential applications in drug delivery (*e.g.* Kimbell et al., 2007; Inthavong et al., 2006, 2008; Schroeter et al., 2006), understanding of pathological conditions (*e.g.* Garcia et al., 2007) and investigation of surgical consequences or objective quantification of surgical outcome (Lindemann et al., 2005b; Zhao et al., 2006) indicate the significance, and some of the potential benefits, of more realistic nasal airflow modelling. In all cases, deficiencies in the current state of modelling, such as unknown parameters and over-simplifying assumptions, are recognised to cause significant limitations in interpretation.

Furthermore, there is a paucity of detailed direct *in vivo* measurements with which model predictions can be compared directly and tested for validity. Such validation of predictions, for instance globally by rhinomanometry, but preferably with distributed, regional measurements of other quantities, such as temperature or particle deposition, would be invaluable. It is appreciated that such measurements pose considerable challenges to the experimental physiologist, but without detailed comparisons, physical model and computational studies are left ungrounded.

Much effort is concerned with improving model definition. There is, however, considerable work to be done in the area of rational geometry characterisation, which should aim to provide the ability to describe both model and real, subject-specific, normal and pathological geometries objectively and comparatively. It could also facilitate the task of introducing architectural simplifications into models that can assist in elucidating the underlying mechanics. Considerable effort is still involved in the translation of *in vivo* data to a model, and progress in automating this process would be of great benefit. Non-invasive rapid and high-resolution imaging could be applied to determine regional variation in passageway geometry over the time course of the nasal cycle, and possibly in due course, other more rapid dynamic geometry changes.

Dynamic flow modelling and coupling to the rest of the respiratory tract (which has not been considered directly in this review) is clearly an important area to explore in depth for many reasons. In particular, future flow modelling needs to assess the significance of unsteadiness within the structure of the flow with regard to mixing and transport processes within the nose, as well as the details of overtly transient processes such as sniffing. The cyclical nature of the inspiratory–expiratory process will influence the definition of input conditions in the region and appropriate boundary conditions derived from modelling of the distal regions are needed.

Modelling studies, particularly computational ones, are capable of generating vast amounts of experimental data that can become confusing, or at best hard to assimilate. In order to make good use of such data, it is important to decide very carefully what is desired of the model being studied, and what is the least amount of data required to answer carefully posed, mechanistic questions that are appropriate to the physiologically based topic being investigated. Therefore, it would be helpful if investigators could develop rational methods of data presentation that enable objective, preferably quantitative, comparison with studies by others. This need brings together the matter of rational geometry description with improved focus and discipline in the generation of functional mechanical and physiologically related data outputs. It will provide a significant challenge to modellers in the future.

Acknowledgements

We are indebted to the Biotechnology and Biological Sciences Research Council (BBSRC) who funded this research (E18557 and BB/E02344/1), and to the EPSRC equipment loan pool, Oxford Lasers, the HPCx national computing resource and Fluent Ltd. for additional support. We are grateful for the advice of Mr. N. Tolley of the ENT department of St. Mary's Hospital in Paddington, and for the assistance in model segmentation of Dr. R. Almeyda, formerly of the same ENT department. We also express our thanks to the Radiology Department at that hospital for CT validation of the fabrication process used to create replica models.

References

Bailie, N., Hanna, B., Watterson, J., Gallagher, G., 2006. An overview of numerical modelling of nasal airflow. Rhinology 44 (1), 53–57.
Blum, H., 1967. A transformation for extracting new descriptors of shape. In: Models for the Perception of Speech and Visual Form. M.I.T. Press, pp. 362–380.
Brucker, C., Park, K., 1999. Experimental study of velocity fields in a model of human nasal cavity by DPIV. In: Banerjee, S., Eaton, K. (Eds.), Proceedings 1st International Symposium on Turbulence and Shear Phenomena. September, 12–15, Begell House, Santa Barbara, California, pp. 831–836.
Cakmak, O., Coskun, M., Celik, H., Buyuklu, F., Ozluoglu, L.N., 2003. Value of acoustic rhinometry for measuring nasal valve area. Laryngoscope 113, 295–302.
Carey, J.W., Steegmann, A.T.J., 1981. Human nasal protrusion, latitude, and climate. Am. J. Phys. Anthropol. 56, 313–319.
Chung, S.K., Kim, S.K., 2008. Digital particle image velocimetry studies of nasal airflow. Respir. Physiol. Neurobiol..
Churchill, S.E., Shackelford, L.L., Georgi, J.N., Black, M.T., 2004. Morphological variation and airflow dynamics in the human nose. Am. J. Hum. Biol. 16, 625–638.
Cole, P., 2000. Biophysics of nasal airflow: a review. Am. J. Rhinol., 245–249.
Cotter, C.J., 2008. The variational particle-mesh method for matching curves. J. Phys. A. 41 344003 (18 pp.) doi:10.1088/1751-8113/41/34/344003.
Croce, C., Fodil, R., Durand, M., Sbirlea-Apiou, G., Caillibotte, G., Papon, J.F., Blondeau, J.R., Coste, A., Isabey, D., Louis, B., 2006. In vitro experiments and numerical simulations of airflow in realistic nasal airway geometry. Ann. Biomed. Eng. 34, 997–1007.
Doorly, D.J., Taylor, D.J., Franke, P., Schroter, R.C., 2008a. Experimental investigation of nasal airflow. Proc. Inst. Mech. Eng. H: J. Eng. Med. 222, 439–453, doi:10.1243/09544119jeim330.
Doorly, D.J., Taylor, D.J., Gambaruto, A.M., Schroter, R.C., Tolley, N., 2008b. Nasal architecture: form and flow. Philos. Trans. R. Soc. A 366, 3225–3246, doi:10.1098/rsta.2008.0083.
Eccles, R., 2000. Nasal airflow in health and disease. Acta Otolaryngol. 120 (5), 580–595.

Elad, D., Naftali, S., Rosenfeld, M., Wolf, M., 2006. Physical stresses at the air-wall interface of the human nasal cavity during breathing. J. Appl. Physiol. 100, 1003–1010.
Elad, D., Wolf, M., Keck, T., 2008. Air-conditioning in the human nasal cavity. Respir. Physiol. Neurobiol..
Finck, M., Hanel, D., Wlokas, I., 2007. Simulation of nasal flow by lattice Boltzmann methods. Comput. Biol. Med. 37, 739–749.
Fodil, R., Brugel-Ribere, L., Croce, C., Sbirlea-Apiou, G., Larger, C., Papon, J.F., Delclaux, C., Coste, A., Isabey, D., Louis, B., 2005. Inspiratory flow in the nose: a model coupling flow and vasoerectile tissue distensibility. J. Appl. Physiol. 98, 288–295.
Franke, V.E., Franke, P.T., Doorly, D.J., Schroter, R.C., Giordana, S., Almeyda, R., 2005. Computational modelling of flow in the nasal cavities. In: Proceedings of the ASME SBC05 Summer Bioengineering Meeting, June 22–26, 2005, Colorado, USA.
Gambaruto, A.M., 2007. Form and flow in anatomical conduits: bypass graft and nasal cavity. Ph.D. Thesis, Department of Aeronautics, Imperial College London.
Gambaruto, A.M., Taylor, D.J., Doorly, D.J., 2008. Modelling nasal airflow using a Fourier descriptor representation of geometry. Int. J. Numer. Methods Fluids, doi:10.1002/fld.1866.
Garcia, G.J.M., Bailie, N., Martins, D.A., Kimbell, J.S., 2007. Atrophic rhinitis: a CFD study of air conditioning in the nasal cavity. J. Appl. Physiol. 103, 1082–1092.
Girardin, M., Bilgen, E., Arbour, P., 1983. Experimental study of velocity fields in a human nasal fossa by laser anemometry. Ann. Otol. Rhinol. Laryngol. 92, 231–236.
Guilmette, R.A., Birchall, A., Jarvis, N.S., 1998. Effect of uncertainty in nasal airway deposition of radioactive particles on effective dose. Radiat. Prot. Dosim. 79 (1–4), 245–248.
Hahn, I., Scherer, P.W., Mozell, M.M., 1993. Velocity profiles measured for airflow through a large-scale model of the human nasal cavity. Model. Physiol. 75, 2273–2287.
Hanif, J., Jawad, S.S.M., Eccles, R., 2000. The nasal cycle in health and disease. Clin. Otolaryngol. 25 (6), 461–467.
Hopkins, L.M., Kelly, J.T., Wexler, A.S., Prasad, A.K., 2000. Particle image velocimetry measurements in complex geometries. Exp. Fluids 29 (1), 91–95.
Hornung, D.E., Leopold, D.A., Youngentob, S.L., Sheehe, P.R., Gagne, G.M., Thomas, F.D., Mozell, M.M., 1987. Airflow patterns in a human nasal model. Arch. Otolaryngol. Head Neck Surg. 113, 169–172.
Horschler, I., Brucker, C., Schroder, W., Meinke, M., 2006. Investigation of the impact of the geometry on the nose flow. Eur. J. Mech. Fluids 25, 471–490.
Horschler, I., Meinke, M., Schroder, W., 2003. Numerical simulation of the flow field in a model of the nasal cavity. Comput. Fluids 32, 39–45.
Inthavong, K., Tian, Z., Li, H., Tu, J., Yang, W., Xue, C., Li, C., 2006. A numerical study of spray particle deposition in a human nasal cavity. Aerosol Sci. Technol. 40 (11), 1034–1045.
Inthavong, K., Tiana, Z.F., Tua, J.Y., Yangb, W., Xuec, C., 2008. Optimising nasal spray parameters for efficient drug delivery using computational fluid dynamics. Comput. Biol. Med. 38 (6), 713–726.
Ishikawa, S., Nakayama, T., Watanabe, M., Matsuzawa, T., 2006. Visualization of flow resistance in physiological nasal respiration. Arch. Otolaryngol. Head Neck Surg. 132, 1203–1209.
Jain, A.K., 1988. Fundamentals of Digital Image Processing. Prentice-Hall International Editions, pp. 370–374, 382–383.
Kelly, J.T., Asgharian, B., Kimbell, J., Wong, B.A., 2004a. Particle deposition in human nasal airway replicas manufactured by different methods. Part I. Inertial regime particles. Aerosol Sci. Technol. 38, 1072–1079.
Kelly, J.T., Asgharian, B., Kimbell, J., Wong, B.A., 2004b. Particle deposition in human nasal airway replicas manufactured by different methods. Part II. Ultrafine particles. Aerosol Sci. Technol. 38, 1072–1079.
Keyhani, K., Scherer, P.W., Mozell, M.M., 1995. Numerical simulation of airflow in the human nasal cavity. J. Biomech. Eng. 117, 429–441.
Keyhani, K., Scherer, P.W., Mozell, M.M., 1997. A numerical model of nasal odorant transport for the analysis of human olfaction. J. Theor. Biol. 186 (3), 279–301.
Kim, J.K., Yoon, J.H., Kim, C.H., Nam, T.W., Shim, D.B., Shin, H.A., 2006. Particle image velocimetry measurements for the study of nasal airflow. Acta Otolaryngol. 126 (3), 282–287.
Kim, S.K., Chung, S.K., 2004. An investigation on airflow in disordered nasal cavity and its corrected models by tomographic PIV. Meas. Sci. Technol. 15, 1090–1096.
Kimbell, J.S., Segal, R., Asgharian, B., Wong, B.A., Schroeter, J.D., Southall, J.P., Dickens, C.J., Brace, G., Miller, F.J., 2007. Characterization of deposition from nasal spray devices using a computational fluid dynamics model of the human nasal passages. J. Aerosol Med. 20, 59–74.
Kleven, M., MeLaaen, M.C., Reimers, M., Rotnes, J.S., Aurdal, L., Djupesland, P.G., 2005. Using Computational Fluid Dynamics (CFD) to improve the bi-directional nasal drug delivery concept. Food Bioprod. Process. 83 (C2), 107–117.
Kobbelt, L., Campagna, S., Vorsatz, J., Seidel, P.H., 1998. Interactive multi-resolution modeling on arbitrary meshes. In: Proceedings of the International Conference on Computer Graphics and Interactive Techniques, pp. 105–114.
Lang, J., 1989. Clinical Anatomy of the Nose, Nasal Cavity and Paranasal Sinuses. George Thieme Verlag, New York.
Lindemann, J., Keck, T., Wiesmiller, K.M., Rettinger, G., Brambs, H.J., Pless, D., 2005a. Numerical simulation of intranasal air flow and temperature after resection of the turbinates. Rhinology 43, 24–28.
Lindemann, J., Brambs, H.J., Keck, T., Wiesmiller, K.M., Rettinger, G., Pless, D., 2005b. Numerical simulation of intranasal airflow after radical sinus surgery. Am. J. Otolaryngol. 26 (3), 175–180.
Lindemann, J., Keck, T., Wiesmiller, K., Sander, B., Brambs, H.J., Rettinger, G., Pless, D., 2004. A numerical simulation of intranasal air temperature during inspiration. Laryngoscope 114, 1037–1041.
Márquez Dorsch, F., Cenjor Español, C., Gutiérrez Fonseca, R., 1996. Acoustic rhinometry in a normal population. Acta Otorrinolaringol. Esp. 47 (2), 121–124.
Mygind, N., Dahl, R., 1998. Anatomy, physiology and function of the nasal cavities in health and disease. Adv. Drug Deliv. Rev. 29 (1/2), 3–12.
Naftali, S., Rosenfeld, M., Wolf, M., Elad, D., 2005. The air-conditioning capacity of the human nose. Ann. Biomed. Eng. 33, 545–553.
Naftali, S., Schroter, R.C., Shiner, R.J., Elad, D., 1998. Transport phenomena in the human nasal cavity: a computational model. Ann. Biomed. Eng. 26, 831–839.
Negus, V., 1958. Comparative Anatomy and Physiology of the Nose and Paranasal Sinuses. F. and S. Livingstone Ltd., Edinburgh/London.
Numminem, J., 2003. Clinical Validation of Rhinometric Measurements, Academic Dissertation. University of Tampere, Tampere, Finland.
Ohki, M., Naito, K., Cole, P., 1991. Dimension and resistance of the human nose: racial differences. Laryngoscope 101, 276–278.
Proctor, D.F., 1977. The upper airways: nasal physiology and defense of the lungs. Am. Rev. Respir. Dis. 115, 97–129.
Proctor, D.F., 1986. Form and function in the upper airways and larynx (Chapter 6). In: Fishman, A.P. (Ed.), The Handbook of Physiology Section 3: The Respiratory System Volume III. Mechanics of Breathing, Part 1. The American Physiological Society, Maryland, pp. 63–73.
Proetz, A.W., 1951. Air currents in the upper respiratory tract and their clinical importance. Ann. Otol. Rhinol. Laryngol. 60, 439–467.
Schreck, S., Sullivan, K.J., Ho, C.M., Chang, H.K., 1993. Correlations between flow resistance and geometry in a model of the human nose. J. Appl. Physiol. 75, 1767–1775.
Schroeter, J.D., Kimbell, J.S., Asgharian, B., 2006. Analysis of particle deposition in the turbinate and olfactory regions using a human nasal computational fluid dynamics model. J. Aerosol Med.—Deposition Clearance and Effects in the Lung 19 (3), 301–313.
Schwab, K.H., v Hagens, G., 1981. Freeze substitution of macroscopic specimens for plastination. Abstract: Sixth European Anatomical Congress. Acta Anat. 111 (12), 399.
Shaida, A.M., Kenyon, G.S., 2000. The nasal valves: changes in anatomy and physiology in normal subjects. Rhinology 38, 7–12.
Shi, H., Kleinstreuer, C., Zhang, Z., 2006. Laminar airflow and nanoparticle or vapor deposition in a human nasal cavity model. ASME J. Biomech. Eng. 128, 697–706.
Shi, H., Kleinstreuer, C., Zhang, Z., 2007. Modeling of inertial particle transport and deposition in human nasal cavities with wall roughness. J. Aerosol Sci. 38, 398–419.
Simmen, D., Scherrer, J.L., Moe, K., Heinz, H., 1999. A dynamic and direct visualization model for the study of nasal airflow. Arch. Otolaryngol. Head Neck Surg. 125, 1015–1021.
Sonka, M., 1995. Image Processing, Analysis and Machine Vision. Chapman and Hall Computing, pp. 422–442, 192–242.
Subramaniam, R.P., Richardson, R.B., Morgan, K.T., Kimbell, J.S., 1998. Computational fluid dynamics simulations of inspiratory airflow in the human nose and nasopharynx. Inhal. Toxicol. 10 (2), 91–120.
Suzina, A.H., Hamzah, M., Samsudin, A.R., 2003. Active anterior rhinomanometry analysis in normal adult Malays. J. Laryngol. Otol. 117, 605–608.
Swift, D.L., Proctor, D.F., 1977. Access of air to the respiratory tract. Respir. Defense Mech., 63–91.
Taylor, D.J., Franke, V.E., Doorly, D.J., Schroter, R.C., 2005. Airflow in the human nasal cavity. In: Proceedings of the ASME SBC05 Summer Bioengineering Meeting, June 22–26, 2005, Colorado, USA.
Taylor, D.J., Doorly, D.J., Schroter, R.C., 2008a. Inflow boundary profile effects on numerical simulations of nasal airflow, Imperial College Aeronautics Report IC 08-01. Extended account also to be published.
Taylor, D.J., Gambaruto, A.M., Tebutt, G., Doorly, D.J., Schroter, R.C., 2008. Computational simulation of nasal airflow: convergence and sensitivity. To be published.
von Hagens, G., Tiedemann, K., Kriz, W., 1987. The current potential of plastination. Anat. Embryol. 175, 41–421.
Weeks Jr., A.R., 1996. Fundamentals of Electronic Image Processing. SPIE/IEEE Series on Image Science and Engineering, pp. 333–359, 452–470.
Weinhold, I., Mlynski, G., 2004. Numerical simulation of airflow in the human nose. Eur. Arch. Otorhinolaryngol. 261, 452–455.
Wen, J., Inthavong, K., Tu, J., Wang, S., 2008. Numerical simulations for detailed airflow dynamics in a human nasal cavity. Respir. Physiol. Neurobiol. 161 (2), 125–135.
Wexler, D., Segal, R., Kimbell, J., 2005. Aerodynamic effects of inferior turbinate reduction computational fluid dynamics simulation. Arch. Otolaryngol. Head Neck Surg. 131, 1102–1107.
Wolf, M., Naftali, S., Schroter, R.C., Elad, D., 2004. Air-conditioning characteristics of the human nose. J. Laryngol. Otol. 118, 87–92.
Zhang, Z., Kleinstreuer, C., 2004. Airflow structures and nano-particle deposition in a human upper airway model. J. Comput. Phys. 198, 178–210.
Zhao, Z., Scherer, P.W., Hajiloo, S.A., Dalton, P., 2004. Effect of anatomy on human nasal air flow and odorant transport patterns: implications for olfaction. Chem. Senses 29, 365–379.
Zhao, K., Dalton, P., Yang, G.C., Scherer, P.W., 2006. Numerical modeling of turbulent and laminar airflow and odorant transport during sniffing in the human and rat nose. Chem. Senses 31 (2), 107–118.